Characterization of Swirling Flows in a Partly Open Cylinder

M. Imoula[1], R. Saci[1], B. Benkoussas[1] and R. Gatignol[2]

[1] Lab "LDMV", University of Boumerdes / Algérie x
[2] Institut Jean Le Rond d'Alembert, Université Pierre et Marie Curie et CNRS, Paris 05, France

†Corresponding Author Email: *hamidsaci2015@gmail.com*

ABSTRACT

A partly open vertical disk-cylinder system, with an annular top lid, is used to model numerically the characteristics of axisymmetric swirling flows with stagnation and associated flows reversal; commonly referred to as vortex breakdown. The flows are driven by the bottom disk uniform rotation and controlled by the competition between the no-slip and stress-free surface conditions applied at the top. Depending on the radial extent of the free surface, distinct regions of toroidal, corner and on-axis vortex type flows were identified and mapped into a state diagram then discussed. In addition, the impact of the cavity aspect ratio on the onset conditions of stagnation and breakdown was highlighted. Moreover, the study explored the influence of a diffusion driven meridian circulation, induced by the sidewall differential rotation, which is revealed to constitute an effective non intrusive kinematic means of flow control.

Keywords: Cylinder; Lid radius-ratio; Stress-free surface; Vortex breakdown; Differential rotation.

NOMENCLATURE

H	height	Γ	angular momentum (circulation)
k	thermal diffusivity coefficient	Λ_h	cavity aspect ratio
Pr	Prandlt number	Λ_r	lid radius ratio
R	radius	υ	fluid kinematic viscosity coefficient
Re	rotational Reynolds number	Ψ	stream function
r_i	inner radius	Ω	disk rotation rate
S	sidewall rotation rate ratio	Ω_b	bottom disk rotation rate
		Ω_l	cylindrical sidewall rotation rate

1. INTRODUCTION

Disk-cylinder systems constitute benchmark devices to model certain fundamental aspects of hydrodynamics, which involve swirling flows with stagnation and associated flow reversal; frequently encountered in practical application (Lucca *et al*. 2001; Herrada *et al*. 2014). They present well defined boundary conditions and involve minimum flow control parameters which, to some extent, render them amenable to numerical modeling.

The characteristics of confined vortex flows depend strongly on the boundary conditions. Spohn *et al*. (1993, 1998) explored the case when a rigid cover of a vertical cylinder is replaced by a free surface and conducted extensive experimental visualizations to determine the characteristics of the

model flow driven by the bottom disk uniform rotation. Their findings evidenced the sensitivity of the free surface and covered new aspects of flow topology in comparison with the rigid cover case; in particular, the occurrence of vortex rings and toroidal vortices attached to the free surface. Besides, they established a detailed flow-regime diagram which mapped distinct breakdown regions in steady and oscillatory flow regimes; based on the couple of main parameters (Γ, Re) where $\Gamma = H/R$ (height/radius) is the cavity aspect ratio and $Re = \Omega R^2/\upsilon$ the rotational Reynolds number ; Ω and υ being the disk rotation rate and fluid kinematic viscosity coefficient respectively. Numerically, Daube (1991) performed axisymmetric time-dependent simulations, assuming flat free surface, which predicted the occurrence of certain weak toroidal flows, not observed in the

experiments. Spohn *et al.* (1993, 1998) pioneering work motivated numerous subsequent numerical investigations; most of which considered non deformable and stress free surface conditions. Of note, Lopez (1995, 2004) demonstrated that steady free surface toroidal vortex structures can be generated under reflection symmetry conditions; analogous to those induced by the exact co-rotation of coaxial disks shrouded by a stationary sidewall. Piva *et al.* (2005), restricted the rotation to a central part of the end disk while maintaining the remaining annular part sealed to the stationary sidewall; concluding that the no-slip conditions on the annular periphery altered considerably the flow topology and controlled efficiently the formation of the vortex structures. An analogous geometry was explored by Yu *et al.* (2007) to characterize by simulation the steady flow patterns in micro-biorectors; highlighting the strong influence of the cylinder-disk ratio to control the formation of the desired vortex breakdown which ensures favorable environment for cell structure. Serre *et al.* (2007) performed non-linear 3D computations and transition to time-dependent regimes in the case of a deep cavity (*H/R* = 4) ; concluding that the free surface conditions promote the onset of unsteadiness, with an estimate of a critical Reynolds number 15% lower than that obtained in the rigid cover case. Without resorting to any symmetry properties at the surface, Bouffanais and Jacono (2009) carried out a series of computations, considering flow models with flat and moving free-surface in the transitional regime. They reported a significant disagreement between their findings and those presented by Piva *et al.* (2005) who based their model on first order approximations as regards to surface deflection. When a stationary thin rod is added along the cavity axis, Cabeza *et al.* (2010) showed that the critical Reynolds number for the occurrence of vortex breakdown decreases over an initial small range of the rod radius ratio while an increase evidenced outside this range. More recently, Kahouadji *et al.* (2014), performed experimental and axisymmetric numerical investigations to model the free surface shape. They employed curvilinear coordinates transformation associated with an iterative process to simultaneously solve the equations of motions under zero normal stress condition and achieved good agreement with experiments in the case of large surface deflection.

Flows in rotating cylindrical pools, controlled by the differential rotation of a small disk mounted on the surface, were recently studied by Wu *et al.* (2013) who considered 3D numerical simulations in steady and oscillatory regimes. Their results revealed the strong combined impact of the rotating disk radius ratio and the cavity aspect ratio on the flow topology and transition regimes.

In the same context, the work reported here is numerical and concerns the axisymmetric flows driven by the bottom disk rotation of a disk-cylinder system with partly open surface. It is structured into three main sections; the first being devoted to a review of selected past works. The next section sets the physical problem, describes the model equations and boundary conditions as well as the methodology

of solution. The last section provides the results and discussion of three model flows. In particular, for validation, the first considers the well established configuration of a fully open cavity with rotating bottom. This is extended to the geometry with a partly free surface to highlight the flow sensitivity to the lid radius ratio. Then, the sidewall differential rotation is implemented as a kinematic means to control the onset of the vortex structures. Finally, concluding remarks summarize the main findings.

2. FORMULATION

2.1 Physical Problem and Control Parameters

Consider a partly open vertical cylinder of height H and radius R, filled with an incompressible viscous fluid of kinematic viscosity υ and thermal diffusivityk. The cavity is bounded at the top by an annular lid sealed to the sidewall, with inner and outer radii r_i and R, respectively, and a flat non deformable free surface extending over the range $0 \le r < r_i$ as shown schematically in (Fig. 1).

The flow is driven by the bottom disk uniform rotation and/or the cylindrical sidewall at rotation rates Ω_b and Ω_l, respectively.
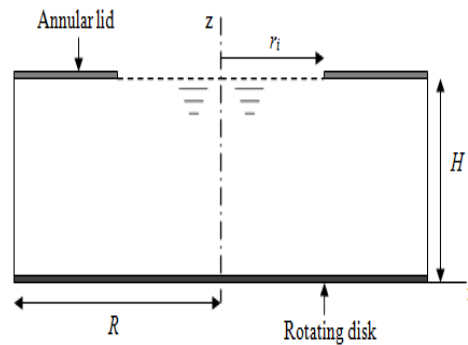

Fig. 1. Schematic of the meridian cross-section of the partly open cylinder.

The governing equations are the unsteady axisymmetric Navier-Stokes equations in cylindrical coordinates (r, θ, z), written in dimensionless form by scaling time, length and velocity with $1/\Omega_b$, R and $\Omega_b R$ respectively. These are then expressed conveniently in a stream function-vorticity formulation (Piva *et al.* 2005; Saci *et al.* 2008); leading to the following non dimensional velocity field which satisfies continuity and the corresponding vorticity field, in terms of the stream function ψ and angular momentum $\Gamma = u_\theta r$,

$$\vec{V} = (u_r, u_\theta, u_z) = (\frac{1}{r}\frac{\partial \psi}{\partial z}, \frac{\Gamma}{r}, -\frac{1}{r}\frac{\partial \psi}{\partial r})$$

$$\nabla \wedge \vec{V} = (\xi_r, \xi_\theta, \xi_z) = (-\frac{1}{r}\frac{\partial \Gamma}{\partial z}, \frac{1}{r}\nabla^2 \psi, \frac{1}{r}\frac{\partial \Gamma}{\partial r})$$

Here, $\nabla_*^2 = \frac{\partial^2}{\partial r^2} - \frac{1}{r}\frac{\partial}{\partial r} + \frac{\partial^2}{\partial z^2}$ denotes the modified laplacian operator and

$\xi_\theta = \partial u_r / \partial z - \partial u_z / \partial r$.

The dimensionless vorticity and circulation transport equations are respectively,

$$\frac{\partial \xi_\theta}{\partial t} + u_r \frac{\partial \xi_\theta}{\partial r} + u_z \frac{\partial \xi_\theta}{\partial z} - \frac{u_r \xi_\theta}{r} - \frac{2\Gamma}{r^3} \frac{\partial \Gamma}{\partial z} = \frac{1}{Re}\left(\nabla^2 \xi_\theta - \frac{\xi_\theta}{r^2}\right)$$

$$\frac{\partial \Gamma}{\partial t} + u_r \frac{\partial \Gamma}{\partial r} + u_z \frac{\partial \Gamma}{\partial z} = \frac{1}{Re}\left(\nabla^2 \Gamma - \frac{2}{r}\frac{\partial \Gamma}{\partial r}\right)$$

The Poisson equation may be written in the form

$$\nabla^2 \psi - \frac{2}{r}\frac{\partial \psi}{\partial r} = -r\xi_\theta$$

$$\nabla^2 = \frac{\partial^2}{\partial r^2} + \frac{1}{r}\frac{\partial}{\partial r} + \frac{\partial^2}{\partial z^2} \text{ is the laplacian operator.}$$

The main dimensionless physical and geometrical parameters which characterize the flow are the Reynolds number, the cavity aspect ratio, the lid radius ratio and finally the sidewall rotation rate ratio defined respectively as

$$Re = \Omega_b R^2 / u_\theta, \Lambda_h = H / R, \Lambda_r = r_i / R, S = \Omega_l / \Omega_b$$

The Prandlt number is $Pr = \upsilon/k$.

2.2 Boundary Conditions

To solve numerically the resulting dimensionless system of equations in the bulk domain $[0,1] \times [0, \Lambda_h]$ boundary and initial conditions are required. These are based on the no slip conditions applied to solid walls and regularity assumption on the cavity axis. Reflexion symmetry is considered on the partly open surface, assumed flat stress-free, (Herrada *et al.* 2014; Hewitt *et al.* 2008; Saci *et al.* 2008) over the range of the flow parameters considered. Initial conditions consider the fluid at rest and the bottom disk is impulsively rotated to a constant angular speed.

These conditions take explicitly the form:

At the bottom disk:

$$z=0,\ 0 < r < 1,\ \Psi=0,\ \Gamma = r^2,\ \xi_\theta = \frac{1}{r}\frac{\partial^2 \Psi}{\partial z^2}$$

At the sidewall:

$$0 < z < \Lambda_h, r = 1, \Psi = 0, \Gamma = S\,r^2, \xi_\theta = -\frac{1}{r}\frac{\partial^2 \Psi}{\partial r^2}$$

Along the cavity axis:

$$r = 0,\ 0 < z < \Lambda_h,\ \Psi = 0,\ \Gamma = 0,\ \xi_\theta = 0$$

At the top annular lid:

$$z = \Lambda_h, \Lambda_r \le r < 1, \Psi = 0, \Gamma = 0, \xi_\theta = \frac{1}{r}\frac{\partial^2 \Psi}{\partial z^2}$$

At the free surface:

$$z = \Lambda_h, 0 \le r < \Lambda_r, \Psi = 0, \frac{\partial \Gamma}{\partial z} = 0, \xi_\theta = 0$$

2.3 Method of Solution and Validation

The solution algorithm is based on a three level time-marching finite difference scheme, used and tested on confined internal swirling flows with breakdown; which has been extended to account for stress-free surface conditions under reflection symmetry; see Saci *et al.* (2008) for detailed accounts and implementation. With appropriate time and space mesh grids, the time dependent solutions of the circulation and the vorticity transport equations were calculated until an ultimate steady state is essentially reached. Poisson's elliptic equation is iterated at each time level and, subsequently, the azimuthal vorticity component is updated at the walls. Most calculations have been carried out in a uniform mesh grid of $100 \times 100\Lambda_h$ elements with a typical initial time step $\delta t = 10^{-4}$; relaxed as the solution progressed in time. The accuracy of the scheme is first assessed by comparison with the benchmark case of fully open cylinder ($\Lambda_r = 1$) explored experimentally and numerically by Spohn *et al.* (1998) and Piva *et al.* (2005). Besides, for a selected couple of flow parameters, additional check was also done by comparing the ultimate steady solution approached for large times with the solution obtained by solving directly the steady equations, by means of the standard successive over relaxation method.

3. RESULTS AND DISCUSSION

Solutions were considered over the selected ranges of parameters; depending on the cavity aspect ratio and radius ratio:

$$200 \le Re \le 2500, 0.5 \le \Lambda_h \le 2.5, 0 \le \Lambda_r \le 1, -1 \le S \le 1$$

3.1 Flows in an Open-Top Cylinder $(\Lambda_r=1)$

The flow in the configuration corresponding to the particular case $\Lambda_r = 1$, $Pr = 1$ is well documented (Spohn *et al.* 1998; Piva *et al.* 2005; Kahouadji *et al.* 2014) and is described in this section. A primary outward motion is imparted to the viscous fluid by the bottom disk uniform rotation, which results in the development of an Ekman layer. The stationary sidewall imposes kinematics constraints; causing an axial motion towards the free surface and the formation of a shear layer which thickens with increasing height, unlike the case of a rigid top surface model. Along the free surface, neglecting losses by viscous dissipation, the angular momentum is almost conserved. There, fluid spirals radially inwards up to the axial core, with no boundary layer, then flows axially downwards, due to the Ekman pumping on the rotating disk. This results in a large scale anticlockwise meridian circulation which redistributes the angular momentum to the interior and induces a concentrated axial core region. This latter, beyond a threshold rotation rate, breaks and gives rise to a distinct clockwise reverse flow region, of weak intensity, which may be located on the cavity axis (bubble type or on-axis vortex breakdown) between two stagnation points at which the axial velocity component vanishes (Spohn *et al.* 1998). As will be illustrated in the following sections, along the cavity axis, fluid flows upward within the bubble while outside it the primary flow is downward.

It is well established (Spohn *et al.* 1998; Piva *et al.* 2005; Serre *et al.* 2007) that increasing Re causes spontaneously the occurrence of a clockwise toroidal type of reverse flow, attached to the free surface. Further increase of the disk rotation rate causes oscillatory regimes (Serre *et al.* 2007).

When completely detached from the cavity axis, the secondary structure is bounded at the surface by two stagnation circles which intersect the meridian plane to define the free surface stagnation points at which the radial velocity component vanishes. Fluid between these points flows radially outward while the primary flow outside them is inward. It is worth mentioning that the associated azimuthal velocity component frequently displays an inflection point which coincides with the reverse flow region. Besides, the corresponding vortex or circulation lines (lines of constant Γ), not shown for brevity, which indicate the local direction of the vorticity, meet orthogonally the surface considered non deformable and stress-free. Their bending at the free surface in the radial direction, observed with increasing Re, generates an axial gradient of the angular momentum which drives the flow radially and strengthens the meridian circulation. When this latter is large enough the flow stagnates.

In (Fig.2), for the sake of comparison with experiments of Piva and Meiburg (2005), we represent both the right and left meridian streamlines (symmetric with respect to the cavity axis); obtained by modeling the free surface flow characterized by: $\Lambda_r = 1$, $\Lambda_h = 1$ and $Re = 1120$. The flow topology is in a good qualitative agreement with the axisymmetric flow pattern reported in the above reference and obtained by visualization of dye injection. It is also in accord with the selected numerical results of Kahouadji *et al.* (2014). The streamlines depict clearly two distinct axisymmetric regions: a toroidal structure attached to the surface imbedded into an ambient primary meridian flow. The secondary flow is of corner type, characterized by an upstream free surface stagnation point and a downstream point located on the cavity axis.
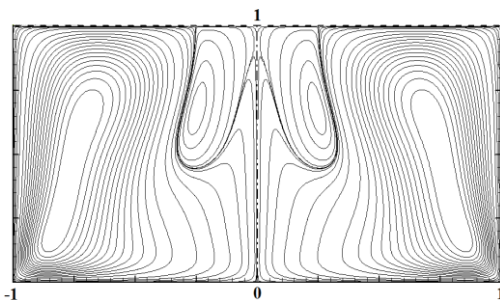

Fig. 2. Meridian streamlines for $\Lambda_r = 1, \Lambda_h = 1, Re = 1120$. In qualitative agreement with experiments of Piva *et al.* (2005).

3.2 Flows in a Partly Open Cavity

As mentioned above, the modified disk-cylinder system is characterized by a top annular lid $(z = \Lambda_h, \Lambda_r \leq r < 1)$ sealed to the cylindrical sidewall, and a partly free surface with radial extent

$0 \leq r < \Lambda_r$. The particular cases $\Lambda_r = 0$ and $\Lambda_r = 1$ correspond respectively to the benchmark configurations of enclosed and fully open cylinder.

To the authors knowledge, the intermediate range $0 < \Lambda_r < 1$ does not appear to have been explored in the literature. The effect of lid radius-ratio is best viewed with reference to (Fig.3); which qualitatively depicts the meridian streamlines for four radius-ratios and selected parameters: $Re = 1250$, $\Lambda_h = 1$. The unit cavity aspect ratio is adopted here for validation with previous experiments carried out in the test case of fully open cavity ($\Lambda_r = 1$). For this couple of parameters, this latter configuration exhibits an axisymmetric toroidal vortex attached to the surface; in qualitative agreement with the findings reported in the literature (Spohn *et al.* 1998; Piva *et al.* 2005). The presence of the annular lid imposes no slip conditions which affect the angular momentum transfer towards the adjacent free surface as well as the radial pressure gradient balance. Consequently, the onset conditions of flow stagnation and breakdown are significantly altered with decreasing Λ_r. In particular, the off-axis toroidal structure moves radially towards the cavity axis to form a corner vortex whose downstream on-axis stagnation point extends axially downwards as clearly illustrated for $\Lambda_r = 0.8; 0.6; 0.4$. A further decrease of Λ_r causes the occurrence of a distinct bubble type vortex breakdown located entirely on the cavity axis as defined in the above section and illustrated in (Fig.3) for $\Lambda_r = 0.3$. A further decrease of Λ_r, over the remaining free surface range, no breakdown occurs as the annular lid no slip condition predominates over the slip condition assumed on the free surface part. This is shown for the selected value $\Lambda_r = 0.2$.

The impact of the radius ratio on the corresponding free surface velocity field is depicted in (Fig.4) for five uniformly spaced values of Λ_r, when $Re = 1250$, $\Lambda_h = 1$. For fixed Λ_r, the swirl and the radial inflow are of the same order of magnitude in the vicinity of the annular lid edge and both intensify radially inward to reach a maximum ($u_{\theta\,max} \gtrsim 2\,u_{r\,max}$) before they decay rapidly towards the cavity axis. Besides, as Λ_r decreases, it is remarked that both $u_{\theta\,max}$ and $u_{r\,max}$ decrease almost linearly and shift toward the cavity axis.

In addition, the associated axial velocity distribution u_z, along the cavity axis, is illustrated (Fig.5), for the same parameters; namely, $Re = 1250$, $\Lambda_h = 1$. It is observed that the velocity component u_z vanishes at each stagnation point before changing sign; indicating a change of axial flow direction which evidences the vortex breakdown occurrence.

Further detailed characteristics of the lid radius ratio effects are remarked in the (Re_c, Λ_r) state diagram of (Fig.6); established on the basis of a series of calculations carried out for the fixed aspect ratio $\Lambda_h = 1$; providing threshold Re_c values for flow stagnation and associated breakdown types. Curves $(c1),(c2),(c3)$ denote the bounding curves for onset of a bubble type, a corner structure and a completely detached toroidal vortex respectively.
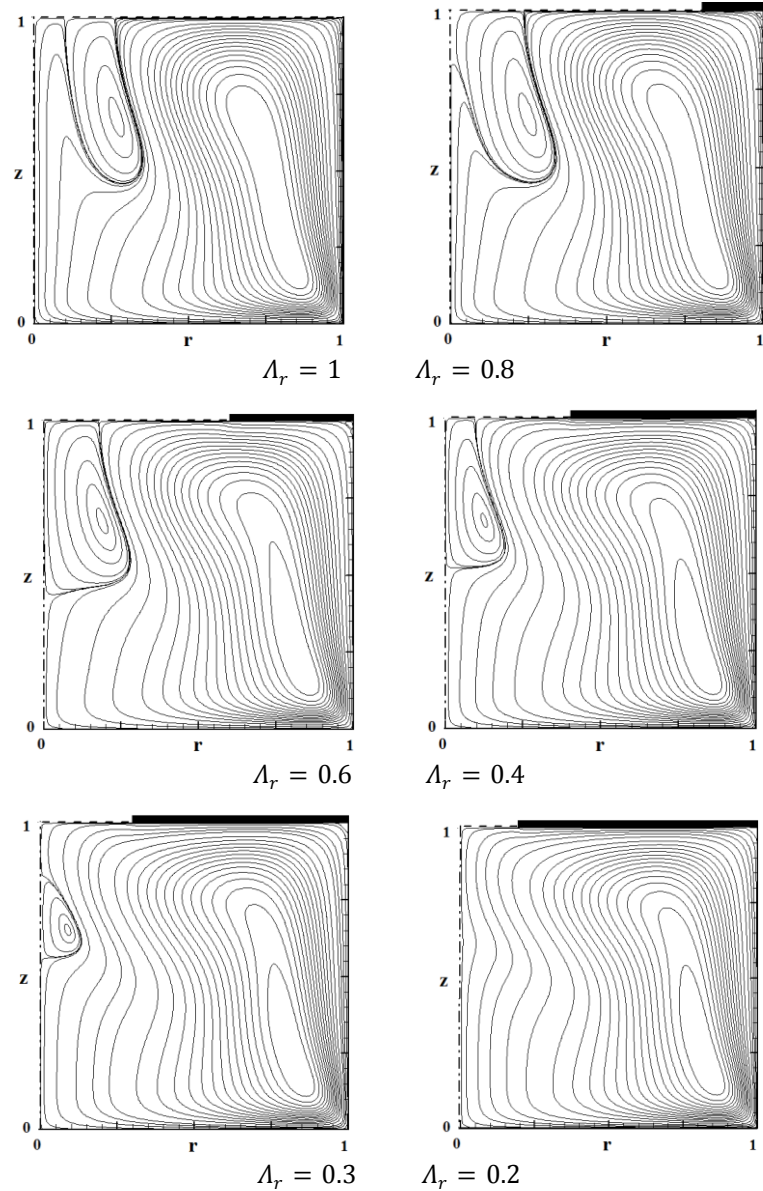
$$\Lambda_r = 1 \qquad \Lambda_r = 0.8$$

$$\Lambda_r = 0.6 \qquad \Lambda_r = 0.4$$

$$\Lambda_r = 0.3 \qquad \Lambda_r = 0.2$$

Fig. 3. Meridian streamlines showing the effect of lid radius-ratio Λ_r ; $Re = 1250, \Lambda_h = 1$ (N.B: the left vertical boundary is the cavity axis).
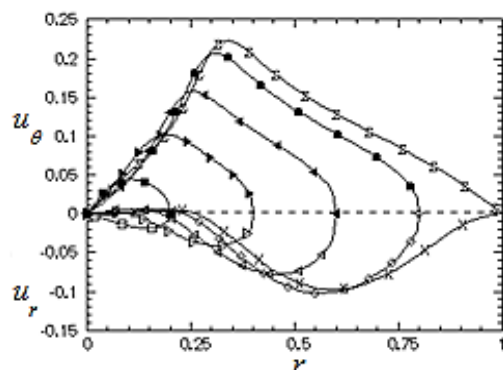

Fig. 4. Radial and tangential velocity distribution at the free surface ; $Re = 1250$, $\Lambda_h = 1$. Curves

□ ▷ ◁ ⊟ ✕

refer to u_r for $\Lambda_r = 0.2, 0.4, 0.6, 0.8, 1$. respectively. The corresponding curves with solid symbols illustrate the profiles of u_θ.
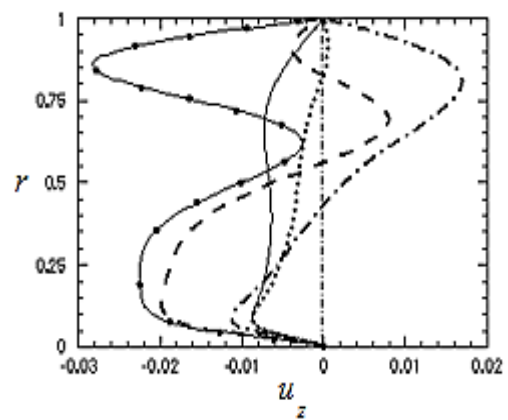

Fig. 5. Axial velocity distribution u_z on the cavity axis for $Re = 1250, \Lambda_h = 1$. Curves

——•—— , — — , — · — · , ········ , ——— **refer to u_z for $\Lambda_r = 0.2, 0.3, 0.6, 0.8, 1$. respectively.**

For the prescribed range of parameters mentioned above, the mapping indicates no breakdown occurrence over the range $0 \leq \Lambda_r < 0.2$ and that the free surface sensitivity intensifies mainly over the intermediate approximate range $0.2 < \Lambda_r < 0.8$; with Re_c lowered sharply by almost five times in the interval $0.2 < \Lambda_r \leq 0.6$. Also remarked in (Fig.6), curves $(c2\ )$ and $(c3)$ are very close one another over the entire range of parameters considered; indicating that the corner vortex pattern occurs within a very sharp range of disk rotation rate. Above curves $(c2\ )$ and $(c3)$ the diagram exhibits a region of toroidal vortex partern over the approximate range $0.4 < \Lambda_r \leq 1$. It is worth mentioning that a vortex formation attached to the free surface is spontaneous and does not necessarily result from a migration process in accord with the statements reported in Hewitt *et al.* (2008) who investigated a related problem of confined swirling flows driven by the co-rotation of co-axial disks.
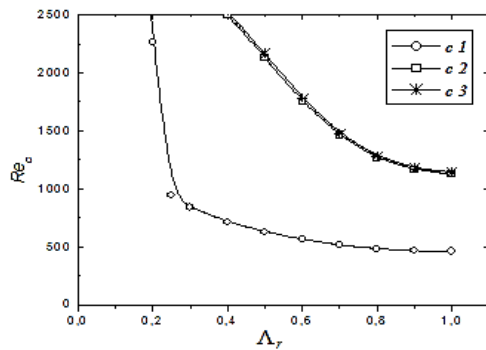

Fig. 6. (Λ_r, Re_c) State diagram for $\Lambda_{\mathrm{h}} = 1$; mapping regions of bubble, corner (very narrow region), and toroidal vortex patterns with lower bounding curves (c1), (c2)and (c3) respectively.

3.3 Effects of the Cavity Aspect Ratio

The sensitivity of the free surface to radius ratio depends strongly on the cavity aspect ratio Λ_h. This is evidenced by the second (Re_c, Λ_r) diagram illustrated in (Fig.7); mapping regions with and without on-axis bubbles and their corresponding bounding curves over the range $0 \leq \Lambda_r \leq 1$ for six aspect ratios; selected in the interval $0.5 \leq \Lambda_h \leq 2.5$. All the results presented in this section for the cases $\Lambda_r = 1$ and $\Lambda_r = 0$ have been validated with the literature (Spohn *et al.* 1998; Piva *et al.* 2005). As mentioned above, we recall that, to our knowledge, the intermediate range $0 < \Lambda_r < 1$ does not appear to have been investigated in previous related studies. However, with decreasing Λ_r a boundary layer forms on the annular lid and one would expect a reduction of angular momentum transfer towards the free surface part which would cause an increase of Re_c and delays the occurrence of reverse flow occurrence. In such a situation we conjecture that the symmetry assumptions would be reasonable; although experimental investigations remain necessary for validation. The established diagram (Fig.7) indicates, as expected, for relatively high aspect ratios; namely, $\Lambda_h = 1.5, 2., 2.5$, a gradual and steady decrease of Re_c with increasing

free surface radial extent over the range $0 \leq \Lambda_r \leq 1$; with an estimate of 15% drop recorded for each Λ_h. The corresponding bounding curves $(c^*4), (c^*5)$ and (c^*6) exhibit each a maximum Re_c reached for $\Lambda_r = 0$; denoting the closed cylinder test case and their regular spacing indicates an almost linear variation of Re_c for fixed lid radius ratio Λ_r. However, for the relatively lower aspect ratios; namely, $\Lambda_h = 0.5, 0.75$ and 1, we observe a very different trend as no breakdown is formed over the range $0 \leq \Lambda_r < 0.15$; revealing a less sensitive free surface than the previous counterparts. In fact, for the prescribed range of aspect ratios, curves $(c^*1), (c^*2)$ and (c^*3) show a very rapid decrease of Re_c with increasing Λ_r over the range $0.15 < \Lambda_r < 1$; with a drop of Re_c by a factor of 10 recorded approximately. Unlike the previous case of relatively higher aspect ratios, it is seen that the bounding curves $(c^*1), (c^*2)$and (c^*3) cross in the interval $0.4 \leq \Lambda_r \leq 0.5$; indicating on one hand a decrease of Re_c with decreasing Λ_h over $0.45 < \Lambda_r \leq 1$, for fixed Λ_r, while the inverse trend is noted on the other hand over the range $0.2 \leq \Lambda_r < 0.45$. This unexpected result evidences the strong dependence of the free surface sensitivity to both lid radius-ratio and cavity aspect ratio. Consequently, the quantitative findings reported for the fully open configuration cannot be systematically extended to a partly open lid system.
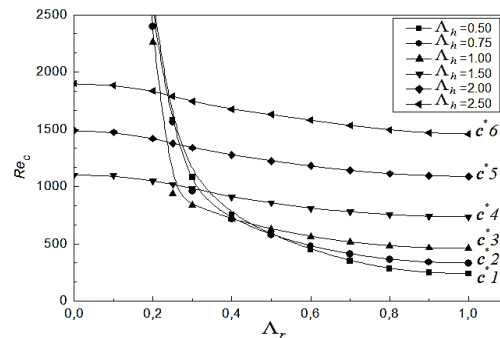

Fig. 7. (Λ_r, Re_c) Diagram, mapping regions of onset of breakdown for six cylinder aspect ratios; namely, $\Lambda_h = 0.5, 0.75, 1, 1.5, 2$ and 2.5. (c*1), (c*2), (c*3), (c*4), (c*5) and (c*6) are the corresponding bounding curves.

3.4 Creeping flow Induced by the Sidewall

In an attempt to investigate on kinematical means of controlling the steady vortex structures described above, we proceed to first explore the creeping motion generated by the sidewall rotation alone, while the bottom disk remained fixed throughout. For the purpose, we select the configuration $\Lambda_h = 1, \Lambda_r = 1$ and define the corresponding Reynolds number $Re_l = \Omega_l R^2 / \upsilon$.

In the absence of the bottom disk, flow would develop towards a state of solid body rotation with no meridian secondary circulation. This is not the case in the finite geometry which imposes no slip conditions on the stationary disk on which develops a Bödewadt type boundary layer. In fact, calculations revealed a radial inflow motion in the vicinity of the

end wall as a result of the unbalanced radial pressure gradient, while an outflow is observed away from it. A relatively slow meridian circulation is thus induced, with upward and downward flow in the interior and in the vicinity of the rotating sidewall, respectively. Compared to the intensity of the primary rotational motion, this type of secondary motion is characterized by a very low velocity magnitude but sufficient enough to prevent the formation of a state of solid rotation as shown in (Fig.8). This latter illustrates the steady three dimensional axial distribution of the velocity field, obtained by solving the full Navier-Stokes equations, resulting from the configuration with rotating sidewall and stationary disk for $Re_l = 0.5$ and $\Lambda_h = 1$ at the chosen radial location r = 0.5.

This specific very low parameter Re_l characterizes typical differential rotation rates within the range explored in the next section, required to control the vortex patterns. (Fig.8) demonstrates the relevant role of the stationary end wall which induces an inward flow on the disk ($u_r < 0$), compared to the cylindrical configuration with infinite extent which leads to solid rotation with no meridian circulation.
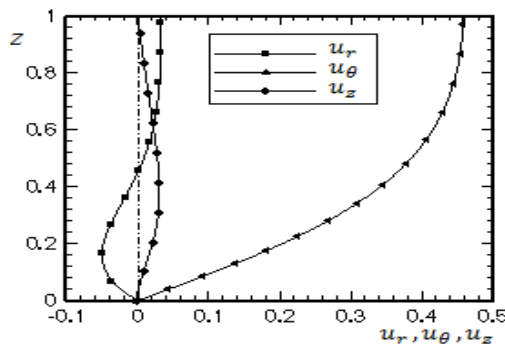

Fig. 8. Axial distribution of the velocity field
(u_r, u_θ, u_z) at $r = 0.5$; $Re_l = 0.5$.

In the configuration with stationary disk and rotating sidewall, the numerical treatment of the full nonlinear Navier-Stokes equations revealed a linear dependence of the flow field on small Re_l . In this limited range, the linearization of the full equations, neglecting nonlinear transport terms, led to the derivation of an analytical solution for the azimuthal velocity component $u_\theta(r, z, t)$, in terms of Bessel series, by the standard method of separation of variables as used, for instance, by Pesso.T, and S. Piva (2015). This is expressed as follows

$$u_\theta(r,z,t) = u_s + 4 \sum_{m \geq l} \sum_{n \geq l} B_{mn} J_1(\alpha_m r) \sin(\beta_n z) exp(-\lambda_{mn}^2 t / Re_l)$$

Where, $u_s(r, z)$ denotes the limiting steady solution given by

$$u_s = r + 2 \sum_{m \geq 1} \frac{J_1(\alpha_m r)}{J_0(\alpha_m)} \left[\frac{\sinh(\alpha_m z) - \sinh(\alpha_m(z - 2\Lambda_h))}{\sinh(2\alpha_m \Lambda_h)} \right]$$

m and n are integers and α_m denotes the mth value of

α for which the Bessel function $J_1(\alpha)$ (of the first kind and first order) is zero. Also,

$$\beta_n = n\pi / 2\Lambda_h, \lambda^2 = \alpha_m^2 + \beta_n^2 ,$$

$$B_{mn} = (1 - (-1)^n) / m\pi J_0(\alpha_m) \lambda^2$$

It is worth mentioning that the steady tangential velocity profile $u_s(r, z)$ shown in (Fig.8) was also deduced using the above analytical expression; which provided an additional check on the accuracy of the numerical approach in the range of linearization.

3.5 Differential Rotation of the Sidewall

The main issue addressed in this section concerns the effects of sidewall differential rotation on the secondary vortex patterns discussed above for the selected test case of a fully open vertical cavity, with aspect ratio $\Lambda_h = 1$. We recall that an additional parameter is introduced for this purpose; namely, the rotation rate ratio = Ω_l / Ω_b ; $-1 \leq S \leq 1$. Although a series of calculations were conducted for a wide range of parameters, the presentation is restricted for brevity to two test cases.

Counter-Rotation

First, we explore a differential counter-rotation of the sidewall on the basic flow which, in accord with Spohn experiments (Spohn *et al.* 1998; Lopez 1995) , exhibits a steady toroidal vortex under the couple of parameters $Re = 1250$, $\Lambda_h = 1$. It is revealed that a very weak counter-rotation rate is sufficient to alter considerably the onset of flow stagnation and associated reverse flow on the free surface; preventing their occurrence as evidenced quantitatively in (Fig.9). This latter shows the radial velocity distribution along the free surface which, under a counter-rotation, directs the flow centrally inward toward the cavity axis.
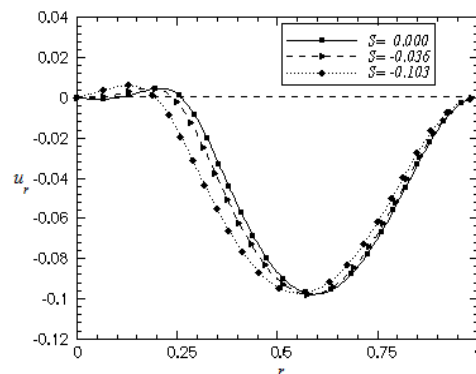

Fig. 9. Radial velocity distribution on the free surface, under effects of counter rotation; Re = 1250, $\Lambda_h = 1$. Rotation rate ratio S = $0, -0.036, -0.103$ as indicated.

Besides, results indicated that an increase of the counter-rotation rate generates flow separation on the sidewall without breakdown; giving rise to a counter-rotating cell whose strength and extent
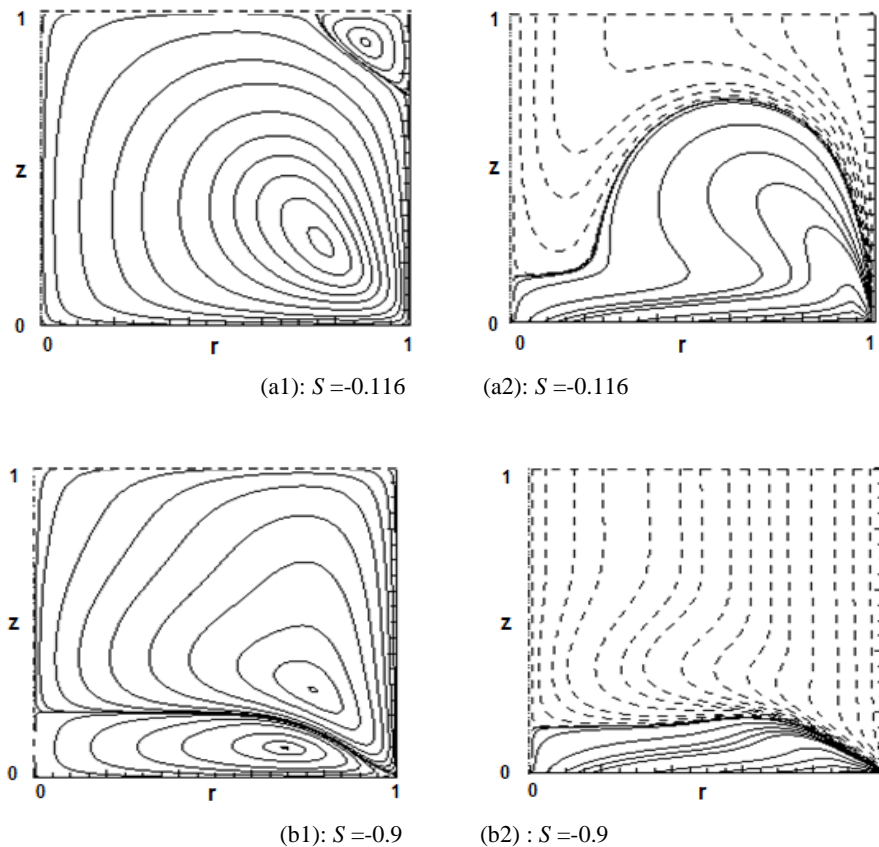
(a1): S =-0.116   (a2): S =-0.116

(b1): S =-0.9   (b2) : S =-0.9

Fig. 10. Effect of counter-rotation; (a1, b1): Streamlines, (a2, b2): iso-circulations for $Re = 600, \Lambda_h = 1$. **The rotation rate ratio S is indicated.**

depend on S. As $|S|$ increases, the cell dominates the bulk flow and confines the end disk effects to a narrow region as displayed in (Fig.10) by the non uniformly spaced meridian streamlines for $Re = 600$, $\Lambda_h = 1$. The corresponding vortex lines (iso-circulations), which indicate the local direction of vorticity, are normal to the free surface and exhibit clearly the two distinct counter-rotating cells (broken lines and solid contours are of opposite sign) separated by a transition curve $\Gamma = 0$ (Fig.10 b1, b2); which tends to coincide with the location of the stagnation curve $\Psi = 0$ (Fig.10 a1, a2) as $|S|$ increases.

Co-Rotation

For the co-rotation case, unlike its above counterpart, calculations revealed that under very weak rotation rate ratios, the diffusion driven circulation induced by the sidewall shear flow enhances the occurrence of axial stagnation points and vortex bubbles while higher rotation rates prevent their occurrence as viewed in (Fig.11), for the selected parameter $Re = 430$, $\Lambda_h = 1$. Starting with a configuration $S = 0$ without any breakdown (Fig.11a), an axial bubble is formed when $S = 0.004$ which widens and migrates towards the surface with increasing $|S|$ before vanishing there, as shown for $S = 0.325$.

4. CONCLUDING REMARKS

Axisymmetric vortex flows, driven by the bottom disk of a partly open-top up-right cylinder, with aspect ratio Λ_h and annular lid radius ratio Λ_r, were numerically studied. The study provided flow characteristics over the intermediate range $0 < \Lambda_r < 1$; extending to some extent the findings generally restricted to the fully open ($\Lambda_r = 1$) and closed ($\Lambda_r = 0$) configurations.

The onset of stagnation and associated flow reversals depend strongly on the competition between the no-slip and stress free surface conditions applied at the cavity top boundary. Numerical predictions showed that increasing the free surface radial extent (Λ_r) promotes the onset of toroidal vortices attached to the free surface but not to its adjacent annular lid. Besides, the impact of the aspect ratio Λ_h was also highlighted over the selected range $0.5 < \Lambda_h \leq 2.5$. In particular, over the sub-range $1 < \Lambda_h \leq 2.5$, a regular and steady decrease of Re_c with increasing Λ_r was recorded. However, for the remaining relatively lower aspect ratios; namely, $0.5 \leq \Lambda_h \leq 1$, no breakdown occurred when $\Lambda_r < 0.15$; while very sharp decrease of Re_c was remarked over $0.15 < \Lambda_r \leq 1$. In addition and unexpectedly, over the sub-range range $0.2 < \Lambda_r < 0.4$, an increase of the aspect ratio renders the surface more sensitive (decrease of Re_c), while the
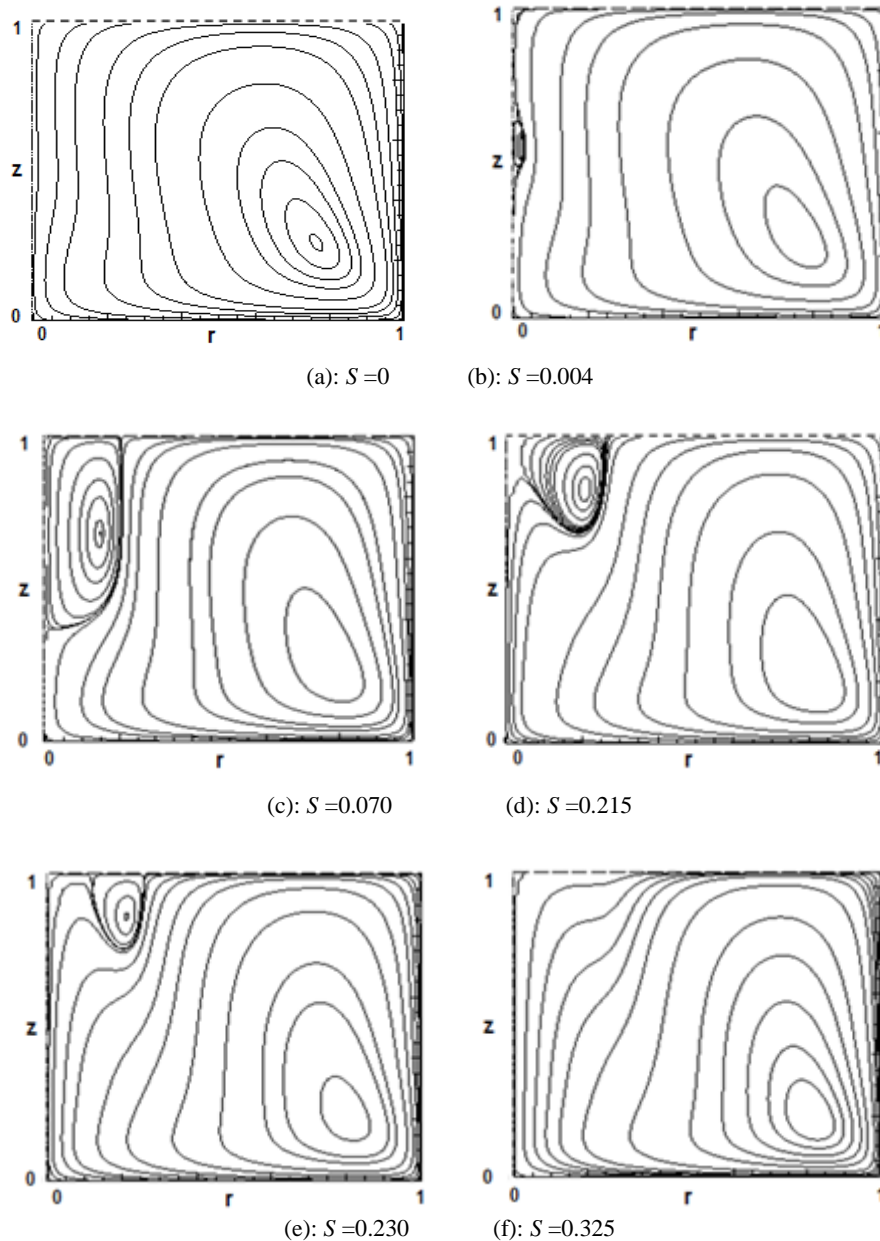
(a): *S* =0   (b): *S* =0.004

(c): *S* =0.070   (d): *S* =0.215

(e): *S* =0.230   (f): *S* =0.325

Fig. 11. Effects of co-rotation. Streamlines pattern when Re = 430, Λ_h = 1; the rotation ratio S is indicated. (N.B: the left vertical boundary is the cavity axis).

opposite effect happens outside this range. Moreover, substantial changes in the flow pattern were evidenced under a differential rotation of the sidewall which induces a meridian circulation of weak intensity but sufficient to suppress (enhance) the flow stagnation under counter-rotation (co-rotation). However, high counter-rotation rates induce sidewall flow separation with the formation of a meridian cell which extends to control the bulk flow and confines the bottom disk effects to a narrow region.

REFERENCES

Bouffanais, R., and D. L. Jacono (2009). Unsteady transitional swirling flow in the presence of a moving free surface. *Phys. Fluids* 21.

Brøns, M., L. K. Voigt and J. N. Sørensen (2001). Topology of vortex breakdown bubbles in a cylinder with a rotating bottom and a free-surface. *J. Fluid Mech.* 428, 133-148.

Cabeza, C., S. Gustavo, C. M. Arturo, B. Italo, V. Sylvana, U. Gabriel and V. Anton (2010). Influence of coaxial cylinders on the vortex breakdown in a closed flow. Euro. *J. of Mechanics (B/Fluids)* 29, 201-207

Daube, O. (1991). Numerical simulation of axisymmetric vortex breakdown in a closed cylinder. *Applied Mathematics* 28, 131-152.

Escudier, M. P. (1984). Observations of the flow

produced in a cylindrical container by a rotating end wall. *Exp. Fluids* 179-186.

Escudier, M. P. (1988). Vortex breakdown, Observations and explanations. *Prog. Aerospace Sci.* 25, 189-229.

Herrada, M. and V. Shtern (2014). Patterns of a creeping water-spout flow. *J. Fluid Mech*. 744, 65-88.

Hewitt, R., T. Mullin, S. Tavener, M. Khan and P. Treacher (2008). Nonlinear vortex development in rotating flows. Philos. *Trans. R. Soc. A* 366, 1317-1329

Kahouadji, L. and L. M. Witkowski (2014). Free surface due to a flow driven by a rotating disk inside a vertical cylindrical tank: Axisymmetric configuration. *Phys. Fluids* 26.

Lopez. J-M (1995). Unsteady swirling flows in an enclosed cylinder with reflectional symmetry. Phys.Fluids 7, 2700-2714.

Lopez, J. M., F. Marques, A. H. Hirsa and R. Miraghaie (2004). Symmetry breaking in Free-surface cylinder flows. *J. Fluid Mech.* 502, 99-126.

Lucca-Negreo, O. and T. O'Doherty (2001). Vortex breakdown: A review. Prog. Energy Comb. *Sci* 27, 431-481.

Mullin, T., J. J. Kobine, S. J. Tavener and K. A. Cliffe (2000). On the creation of stagnation points near straight and sloped walls. *Phys. Fluids* 12(2), 425-431.

Pesso, T. and S. Piva (2015). An analytical solution for the laminar forced convection in a pipe with temperature-dependent heat generation. *J. Fluid Mech.* 8(4), 641-650.

Piva, M. and E. Meiburg (2005). Steady axisymmetric flow in an open cylindrical container with a partially rotating bottom wall. *Phys. Fluids* 17.

Saci, R. and A. Kouadri (2008). Vortex breakdown control in confined swirling flows. *Mécanique and Industries* 9, 51-58.

Serre, E. and P. Bontoux (2007). Vortex breakdown in a cylinder with a rotating bottom and a flat stress-free surface. *Int. J. Heat Fluid Flow* 28, 229-248.

Spohn, A., M. Mory and E. Hopfinger (1993). Observations of vortex breakdown in an open cylindrical container with a rotating bottom. *Exp. Fluids* 14, 70-77.

Spohn, A., M. Mory and E. Hopfinger (1998). Experiments on vortex breakdown in a confined flow generated by a rotating disk. *J. Fluid Mech.* 370, 73-99.

Wu, C. M., Y. R. Li and D. F. Ruan (2013). Aspect ratio and radius ratio dependence of flow pattern. *Phys. Fluids* 25.

Yu, P., T. S. Lee and H. T. Low (2007). Characterization of flow behavior in an enclosed cylinder with a partially rotating end wall. *Phys. Fluids* 19.